energies

MDPI

Article

A Cell-to-Cell Equalizer Based on Three-Resonant-State Switched-Capacitor Converters for Series-Connected Battery Strings

Yunlong Shang, Qi Zhang, Naxin Cui * and Chenghui Zhang *

School of Control Science and Engineering, Shandong University, Jinan 250061, China; shangyunlong@mail.sdu.edu.cn (Y.S.); zhangqi2013@sdu.edu.cn (Q.Z.)

* Correspondence: cuinx@sdu.edu.cn (N.C.); zchui@sdu.edu.cn (C.Z.); Tel.: +86-531-8839-2907 (N.C.); +86-531-8839-5717 (C.Z.)

Academic Editors: Rui Xiong, Hailong Li and Joe (Xuan) Zhou

Received: 23 December 2016; Accepted: 6 February 2017; Published: 11 February 2017

Abstract: Due to the low cost, small size, and ease of control, the switched-capacitor (SC) battery equalizers are promising among active balancing methods. However, it is difficult to achieve the full cell equalization for the SC equalizers due to the inevitable voltage drops across Metal-Oxide-Semiconductor Field Effect Transistor (MOSFET) switches. Moreover, when the voltage gap among cells is larger, the balancing efficiency is lower, while the balancing speed becomes slower as the voltage gap gets smaller. In order to soften these downsides, this paper proposes a cell-to-cell battery equalization topology with zero-current switching (ZCS) and zero-voltage gap (ZVG) among cells based on three-resonant-state SC converters. Based on the conventional inductor-capacitor (LC) converter, an additional resonant path is built to release the charge of the capacitor into the inductor in each switching cycle, which lays the foundations for obtaining ZVG among cells, improves the balancing efficiency at a large voltage gap, and increases the balancing speed at a small voltage gap. A four-lithium-ion-cell prototype is applied to validate the theoretical analysis. Experiment results demonstrate that the proposed topology has good equalization performances with fast equalization, ZCS, and ZVG among cells.

Keywords: battery equalizers; battery management systems; switched-capacitor (SC) converters; zero-voltage gap (ZVG); modularization; electric vehicles (EVs)

1. Introduction

The world is being confronted with unprecedented crises, i.e., the depletion of fossil fuels and the global warming [1]. Energy conservation is becoming of paramount concern to people. In response to the crises, electric vehicles (EVs) have been implemented and are considered to be the inevitable development trend of vehicles for the future [2]. Due to high energy density, long lifetime, and environmental friendliness, lithium-based batteries have been dominating the high power battery packs of EVs [3,4]. However, the terminal voltage of a single lithium battery cell is usually low, e.g., 3.7 V for lithium-ion batteries and 3.2 V for lithium iron phosphate (LiFePO4) batteries [5,6]. In order to meet the demands of the load voltage and power, lithium batteries are usually connected in series and parallel [7]. For example, Tesla Model S uses 7616 lithium-ion 18650 cells connected in series and parallel [8]. Unfortunately, there are slight differences among cells in terms of capacity and internal resistance, which cause the cell voltage imbalance as the battery string is charged and discharged. On the one hand, this imbalance reduces the available capacity of battery packs. On the other hand, it may lead to over-charge or over-discharge for a cell in the battery pack, increasing safety risks. In fact, the most viable solution for this problem might not originate merely from the improvement in the battery chemistry. It also uses suitable power electronics topologies to prevent the cell imbalance, which is known as battery equalization.

During the last few years, many balancing topologies have been proposed, which can be classified into two categories: the passive balancing methods [7,9] and the active balancing methods [10–32]. The passive equalizers employ a resistor connected in parallel with each cell to drain excess energy from the high energy cells [7,9]. These methods have the outstanding advantages of small size, low cost, and easy implementation. However, their critical disadvantages are energy dissipation and heat management problems [7]. To overcome these drawbacks, active cell balancing topologies are proposed, which employ non-dissipative energy-shuttling elements to move energy from the strong cells to the weak ones [7], reducing energy loss. Therefore, active balancing methods have higher balancing capacity and efficiency than the passive equalization ones. They can be further divided into three groups, which are capacitor based [10–18], inductor based [19–21], and transformer based [22–32] methods. Among these active balancing topologies, switched-capacitor (SC) based solutions have the inherent advantages of smaller size, lower cost, simpler control, and higher efficiency. Ref. [10] proposes an SC equalizer for series battery packs. As shown in Figure 1a, one capacitor is employed to shift charge between the adjacent two cells. The capacitor is switched back and forth repeatedly, which diffuses the imbalanced charge until the two cell voltages match completely [10]. The main disadvantage of this structure is the high switching loss. To solve this problem, an automatic equalization circuit based on resonant SC converters is proposed in [15]. As shown in Figure 1b, an inductor L_0 is added to form a resonant inductor-capacitor (LC) converter, which operates alternatively between the charging state and discharging state with zero-current switching (ZCS) to automatically balance the cell voltages [15]. However, it is difficult to apply this topology to the systems with low voltage gap among cells. For example, the voltage difference among lithium-ion battery cells is not allowed to exceed 0.1 V [15]. This small voltage difference causes the Metal-Oxide-Semiconductor Field Effect Transistor (MOSFETs) of the equalizers to fail to conduct, which results in the inevitable residual voltage gap among cells. Moreover, the equalization current becomes smaller as the voltage gap gets smaller, resulting in a very long balancing time.

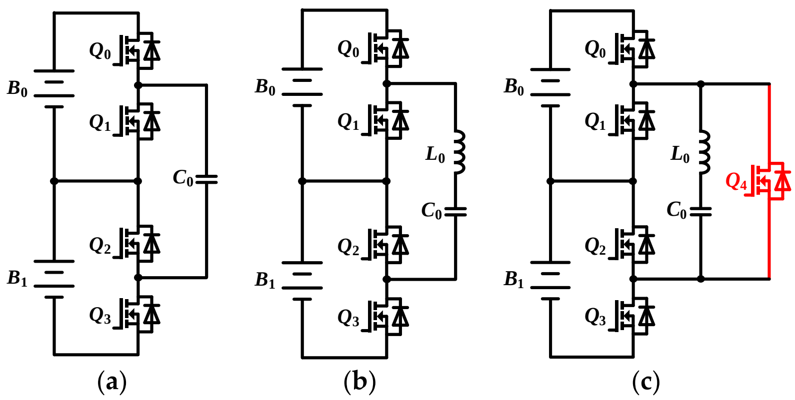

Figure 1. Battery equalizers based on switched-capacitor (SC) converters. (**a**) the classical SC equalizer [10]; (**b**) the resonant SC equalizer [15]; and (**c**) the proposed equalizer based on an inductor-capacitor-switch (LCS) converter.

In order to overcome these problems, a battery equalizer is proposed based on a resonant LC converter and boost converter that offers several major advantages, e.g., ZCS and zero-voltage gap (ZVG) among cells, etc. [16]. However, the balancing efficiency of this topology is strongly related to the voltage conversion ratio, which is expressed as $\eta_e = V_{output}/V_{in}$. The lower the conversion ratio (or the larger the voltage difference), the larger the balancing current, but the lower the balancing efficiency. This means that high efficiency cannot be achieved at a large voltage gap. Ref. [33] proposes a high-efficiency SC converter that decouples the efficiency from the voltage conversion ratio. Ref. [34]

applies the switched-capacitor gyrator to photovoltaic systems, demonstrating ultimate improvement in the power harvesting capability under different insolation levels. Based on these works, the objective of this paper is to introduce an adjacent cell-to-cell battery equalization topology based on three-resonant-state LC converters, with the potential of fulfilling the expectations of high current capability, high efficiency, easy modularization, ZCS, and ZVG among cells. As shown in Figure 1c, except the classical design, an additional switch Q_4 is added to be connected in parallel with the LC tank, which is hereinafter to be referred as the inductor-capacitor-switch (LCS) converter. This structure obtains another resonant current path to release the residual energy stored in the capacitor to the inductor, which lays the foundations to achieve the bi-directional power flow and weakens the couplings of a large voltage gap with low efficiency and a small voltage gap with slow balancing speed.

2. The Proposed Equalizer

2.1. Basic Circuit Structure

As shown in Figure 2, the proposed equalizer can be easily extended to a long series battery string without limit. The architecture consists of n battery cells connected in series and $n-1$ resonant LCS tanks connected in parallel with each two adjacent battery cells, through which energy can be exchanged among all cells.

The proposed equalizer has several major advantages per the following:

(1) The proposed equalizer can achieve ZCS for all MOSFETs, and obtain ZVG among cells.
(2) Due to the other resonant current path, the balancing efficiency is improved at a large voltage gap among cells, and the balancing speed is increased at a small voltage gap.
(3) By changing the parameters of the resonant LCS converter, different balancing speeds can be achieved to meet the requirements of different energy storage devices.
(4) The concept is modular [35], and the topology can be extended to any long series-connected battery strings or individual cells without limit.

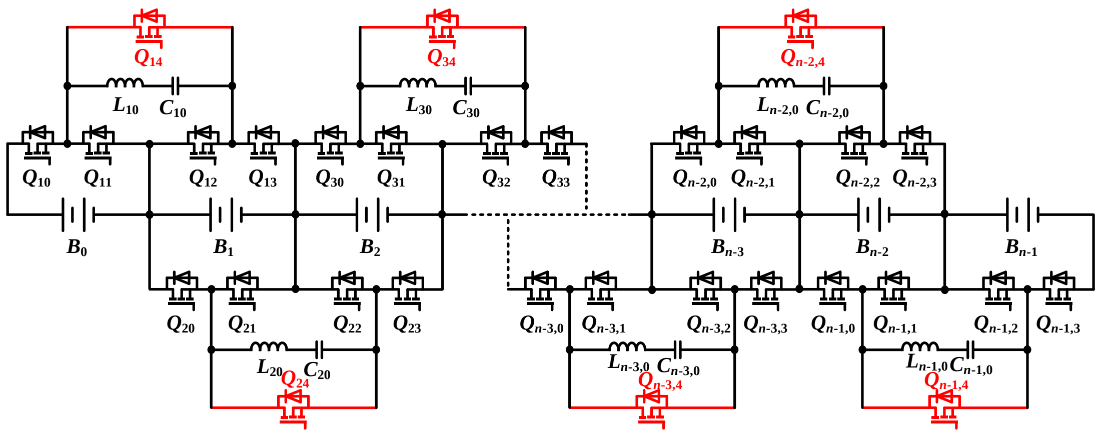

Figure 2. Schematic diagram of the proposed system for n series-connected battery cells.

2.2. Operation Principles

In order to simplify the analysis for the operation states, the following assumptions are made: the proposed equalizer is applied to two cells connected in series, i.e., B_0 and B_1, where B_0 is over-charged and B_1 is undercharged. The operation principles are shown in Figure 3. The switching sequence is set as (Q_0, Q_2), (Q_1, Q_3), and Q_4, as shown in Figure 4. Three resonant states S_1–S_3 are employed to charge, discharge, and release the LC tank, which is connected to a voltage of V_{B0}, V_{B1}, or 0 in each switching state, respectively. Figure 5 shows the theoretical waveforms of the proposed equalizer at $V_{B0} > V_{B1}$.

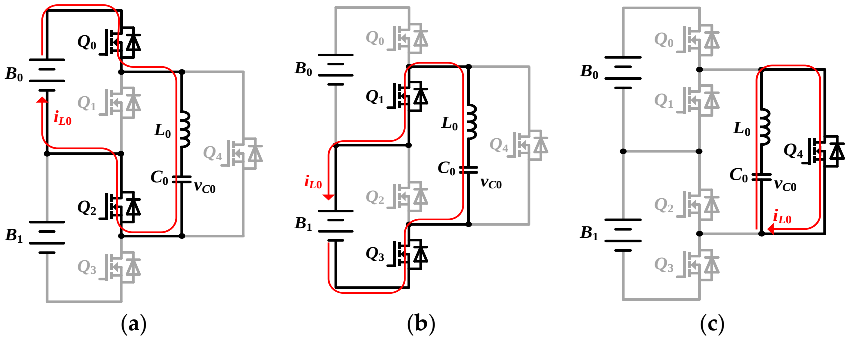

Figure 3. Operating states of the proposed equalizer at $V_{B0} > V_{B1}$. (**a**) charge state S_1; (**b**) discharge state S_2; (**c**) release state S_3.

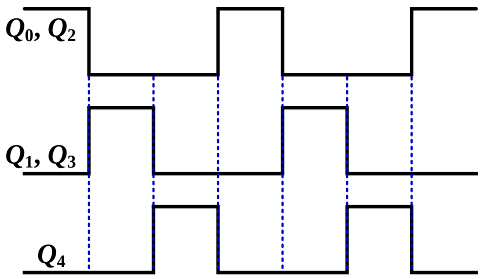

Figure 4. Switching sequences of the proposed equalizer at $V_{B0} > V_{B1}$.

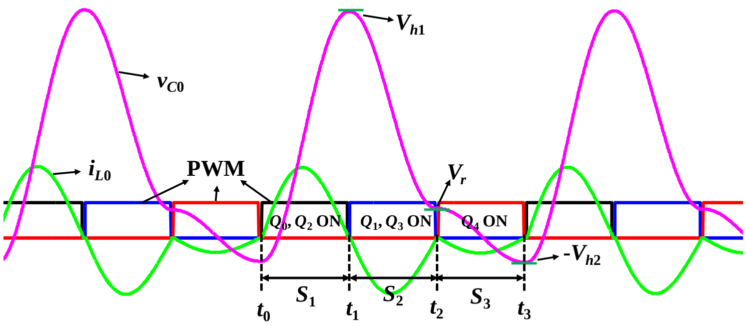

Figure 5. Theoretical waveforms of the capacitor voltage and the resonant current at $V_{B0} > V_{B1}$.

Charge State S_1 [t_0-t_1]: At t_0, switches Q_0 and Q_2 are turned ON with ZCS. The LC tank is connected with B_0 in parallel through Q_0 and Q_2, as shown in Figure 3a. B_0, L_0, and C_0 form a resonant current loop. The capacitor C_0 is charged by B_0. v_{C0} increases from $-V_{h2}$, which is a remnant of C_0 from the last period (see Figure 5). i_{L0} and v_{C0} in this state can be expressed as

$$i_{L0}(t) = \frac{V_{B0} + V_{h2}}{Z_r \cdot \sqrt{1-\rho^2}} \cdot e^{-\rho\omega_n(t-t_0)} \cdot \sin\left[\omega_n \cdot \sqrt{1-\rho^2} \cdot (t-t_0)\right], \tag{1}$$

$$v_{C0}(t) = -V_{h2} + (V_{B0} + V_{h2}) \cdot \left\{1 - \frac{e^{-\rho\omega_n(t-t_0)}}{\sqrt{1-\rho^2}} \cdot \cos\left[\omega_n \cdot \sqrt{1-\rho^2} \cdot (t-t_0)\right]\right\}, \tag{2}$$

where $Z_r = \sqrt{L_0/C_0}$, $\omega_n = 1/\sqrt{L_0 C_0}$, and $\rho = R_S/2Z_r$. R_S represents the equivalent parasitic resistance in each current path.

The charge state ends when i_{L0} crosses zero at $t = t_1$. From Equation (1), the duration of this state is determined by

$$\Delta t = t_1 - t_0 = \frac{\pi}{\omega_n \cdot \sqrt{1-\rho^2}}. \tag{3}$$

At t_1, v_{C0} is positively charged to V_{h1}, which can be given by

$$V_{h1} = v_{C0}(t_1) = (V_{B0} + V_{h2}) \cdot (1 + \frac{e^{-\rho\omega_n \Delta t}}{\sqrt{1-\rho^2}}) - V_{h2}. \tag{4}$$

Discharge State S_2 [t_1-t_2]: At t_1, the switches Q_1 and Q_3 are turned ON with ZCS, connecting B_1 to the resonant LC tank. B_1, L_0, and C_0 form a resonant loop. B_1 is charged by C_0. i_{L0} and v_{C0} in this state are given as

$$i_{L0}(t) = -\frac{V_{h1} - V_{B1}}{Z_r \cdot \sqrt{1-\rho^2}} \cdot e^{-\rho\omega_n(t-t_1)} \cdot \sin\left[\omega_n \cdot \sqrt{1-\rho^2} \cdot (t - t_1)\right], \tag{5}$$

$$v_{C0}(t) = V_{h1} - (V_{h1} - V_{B1}) \cdot \left\{1 - \frac{e^{-\rho\omega_n(t-t_1)}}{\sqrt{1-\rho^2}} \cdot \cos\left[\omega_n \cdot \sqrt{1-\rho^2} \cdot (t - t_1)\right]\right\}. \tag{6}$$

At $t = t_2$, the discharge state ends when i_{L0} drops to zero. The voltage V_r of C_0 at $t = t_2$ is represented by

$$V_r = V_{h1} - (V_{h1} - V_{B1}) \cdot (1 + \frac{e^{-\rho\omega_n \Delta t}}{\sqrt{1-\rho^2}}). \tag{7}$$

Release State S_3 [t_2-t_3]: During this state, the resonant LC tank is short-circuited by turning on the switch Q_4 with ZCS. This releases the residual charge of the capacitor into the inductor and even charges reversely the capacitor C_0, so B_0 can charge C_0 with a large current at the beginning of S_1. This state provides the opportunity to transfer energy from a low voltage cell to a high voltage one, which lays the foundations to achieve ZVG among cells. i_{L0} and v_{C0} in this state are given by

$$i_{L0}(t) = -\frac{V_r}{Z_r \cdot \sqrt{1-\rho^2}} e^{-\rho\omega_n(t-t_2)} \cdot \sin\left[\omega_n \cdot \sqrt{1-\rho^2} \cdot (t - t_2)\right], \tag{8}$$

$$v_{C0}(t) = V_r \cdot \frac{e^{-\rho\omega_n(t-t_2)}}{\sqrt{1-\rho^2}} \cdot \cos\left[\omega_n \cdot \sqrt{1-\rho^2} \cdot (t - t_2)\right]. \tag{9}$$

The release state ends when i_{L0} crosses zero at $t = t_3$. The voltage V_{h2} of C_0 at $t = t_3$ can be expressed as

$$-V_{h2} \equiv v_{C0}(t_3) = V_r \cdot \frac{e^{-\rho\omega_n(t_3-t_2)}}{\sqrt{1-\rho^2}} \cdot \cos\left[\omega_n \cdot \sqrt{1-\rho^2} \cdot (t_3 - t_2)\right] = -\lambda V_r, \tag{10}$$

where

$$\lambda = \frac{e^{-\rho\omega_n \Delta t}}{\sqrt{1-\rho^2}} = \frac{e^{-\pi\rho/\sqrt{1-\rho^2}}}{\sqrt{1-\rho^2}}. \tag{11}$$

By solving Equations (4), (7), and (10), V_{h1}, V_r, and V_{h2} can be calculated as

$$V_{h1} = \frac{V_{B0} + \lambda^2 V_{B1}}{1 - \lambda + \lambda^2}, \tag{12}$$

$$V_r = \frac{V_{B1} - \lambda V_{B1}}{1 - \lambda + \lambda^2}, \tag{13}$$

$$V_{h2} = \frac{\lambda(V_{B1} - \lambda V_{B0})}{1 - \lambda + \lambda^2}. \tag{14}$$

The operating period T is composed of three resonant states, which can be expressed as

$$T = \frac{3\pi}{\omega_n \cdot \sqrt{1-\rho^2}} = \frac{3\pi \cdot \sqrt{L_0 C_0}}{\sqrt{1-\rho^2}}. \quad (15)$$

The direction of the balancing power flowing can be changed by controlling the switching sequences. According to the above analysis, the switching sequence (Q_0, Q_2), (Q_1, Q_3), Q_4 is to deliver energy from B_0 to B_1. In the case of energy transferred from B_1 to B_0, the switching sequence is changed to (Q_1, Q_3), (Q_0, Q_2), Q_4. Figure 6 shows the three consecutive operating states of the proposed equalizer: (a) charge state; (b) discharge state; and (c) release state at $V_{B0} < V_{B1}$. Figure 7 shows the corresponding switching sequence. It can be seen that, by controlling the switching sequence, energy can be delivered between two adjacent cells arbitrarily, by which ZVG between cells can be achieved without any limit.

It is important to note that the release state can also be achieved by turning simultaneously on Q_1 and Q_2 without using Q_4, which results in a reduced MOSFET number but complex control. Figures 8 and 9 show the three consecutive operating states without using Q_4 and the corresponding switching sequences at $V_{B0} > V_{B1}$. Figures 10 and 11 show the three consecutive operating states without using Q_4 and the corresponding switching sequences at $V_{B0} < V_{B1}$. The operation principles of this system are similar to those shown in Figures 3–6 and will not be described here in detail.

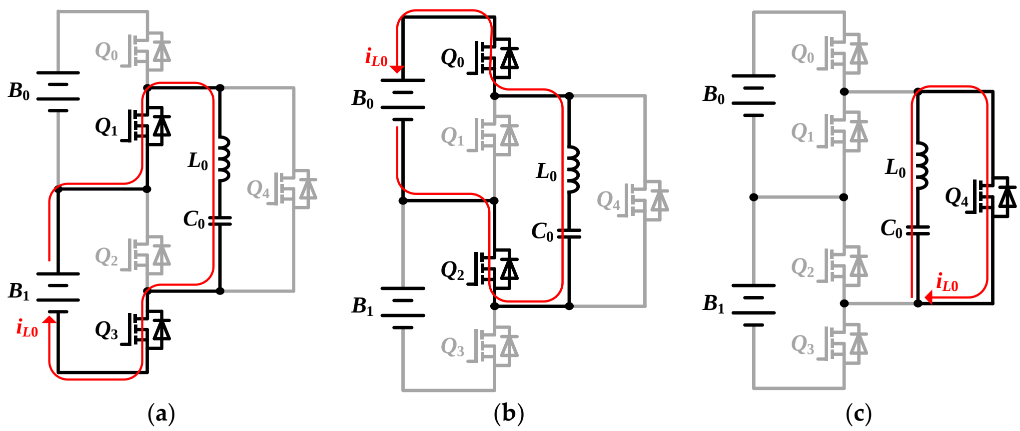

Figure 6. Operating states of the proposed equalizer at $V_{B0} < V_{B1}$. (**a**) charge state; (**b**) discharge state; (**c**) release state.

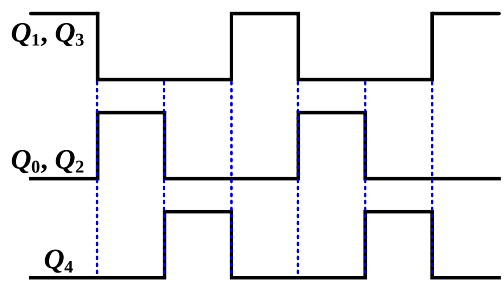

Figure 7. Switching sequences of the proposed equalizer at $V_{B0} < V_{B1}$.

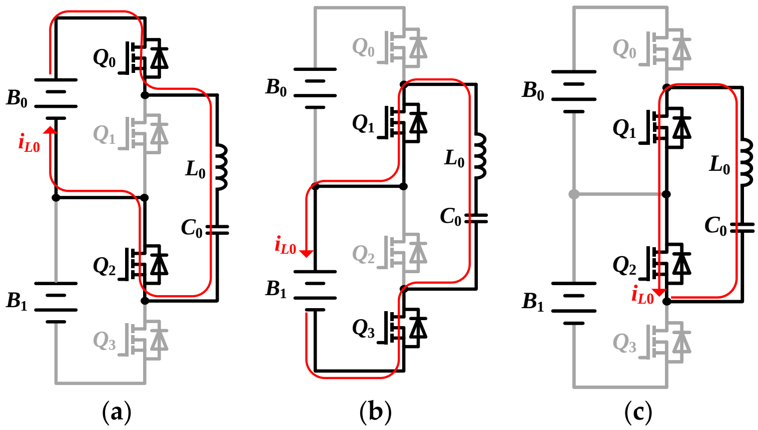

Figure 8. Operating states of the proposed equalizer without using Q_4 at $V_{B0} > V_{B1}$. (**a**) charge state; (**b**) discharge state; (**c**) release state.

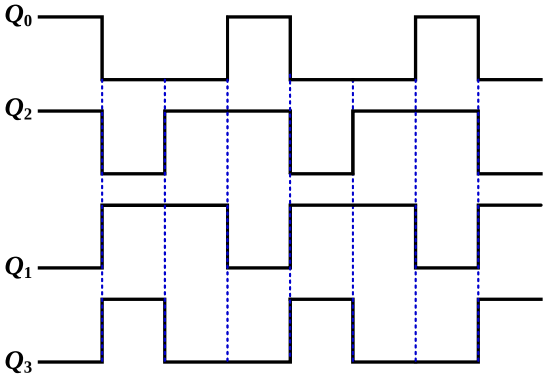

Figure 9. Switching sequences of the proposed equalizer without using Q_4 at $V_{B0} > V_{B1}$.

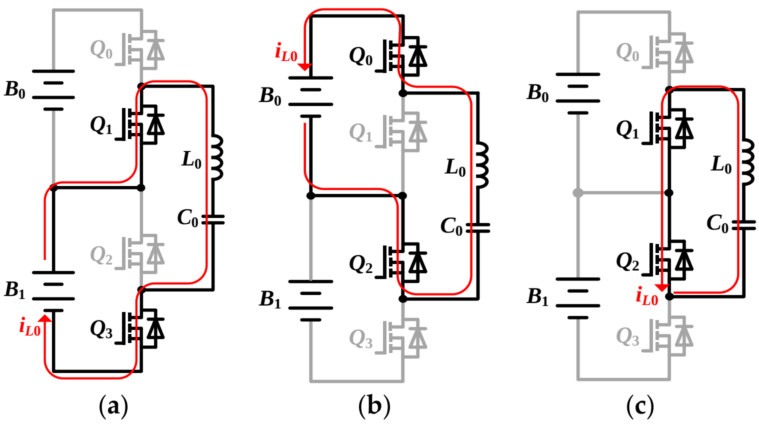

Figure 10. Operating states of the proposed equalizer without using Q_4 at $V_{B0} < V_{B1}$. (**a**) charge state; (**b**) discharge state; (**c**) release state.

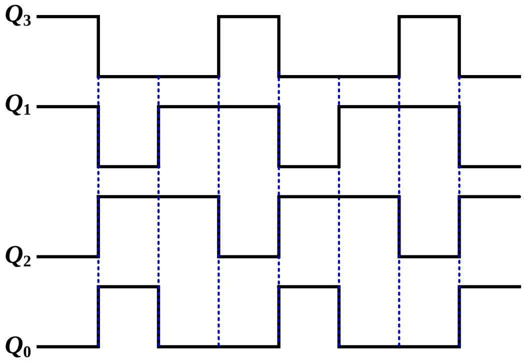

Figure 11. Switching sequences of the proposed equalizer without using Q_4 at $V_{B0} < V_{B1}$.

2.3. Equalizing Power and Efficiency

During one switching period T, the charge delivered to C_0 from B_0 is

$$\Delta Q_D = C_0 \cdot (V_{h_1} + V_{h_2}), \tag{16}$$

and the charge received by B_1 is expressed as

$$\Delta Q_R = C_0 \cdot (V_{h_1} - V_r). \tag{17}$$

Using Equations (12)–(14) and (16), the average power flowing out of B_0 is obtained as

$$P_{avg,D} = \Delta Q_D \cdot V_{B_0} = \frac{V_{B0} \cdot \sqrt{1-\rho^2}}{3\pi Z_r} \times \frac{(1+\lambda) \cdot [(1-\lambda) \cdot V_{B0} + \lambda \cdot V_{B1}]}{1-\lambda+\lambda^2}, \tag{18}$$

and, using Equations (12)–(14) and (17), the average power flowing into B_1 is given as

$$P_{avg,R} = \Delta Q_R \cdot V_{B_1} = \frac{V_{B1} \cdot \sqrt{1-\rho^2}}{3\pi Z_r} \times \frac{(1+\lambda) \cdot [V_{B0} - (1-\lambda) \cdot V_{B1}]}{1-\lambda+\lambda^2}. \tag{19}$$

Based on Equations (18) and (19), the equalization efficiency η_e can be calculated as

$$\eta_e = \frac{P_{avg,R}}{P_{avg,D}} = \frac{V_{B1}}{V_{B0}} \cdot \frac{V_{B0} - (1-\lambda) \cdot V_{B1}}{(1-\lambda) \cdot V_{B0} + \lambda \cdot V_{B1}} \times 100\%. \tag{20}$$

Figure 12 shows the balancing efficiency curves obtained from Equation (20) as a function of the L_0/C_0 ratio, for various R_S, under the conditions of V_{B0} = 3.3 V and V_{B1} = 3.2 V. It can be observed that the efficiency increases as the L_0/C_0 ratio increases or R_S decreases, which show how the coupling of the large voltage gap with low efficiency can be weakened by keeping R_S as low and the L_0/C_0 ratio as high as possible. However, from Equations (1) and (5), it can be concluded that the balancing current would become smaller as the L_0/C_0 ratio increases. Therefore, an appropriate L_0/C_0 ratio (e.g., L_0/C_0 = 10) should be selected in order to achieve a higher balancing efficiency and larger balancing current.

Figure 13 presents the efficiency curve as a function of power at L_0/C_0 = 10 and R_S = 0.18 Ω. The balancing efficiency rises rapidly when the power increases from 0.12 W to 0.5 W and basically stays at a high value when the power increases from 0.5 W to 0.9 W, but decreases slightly when the power increases from 0.9 W to 1.3 W. The peak efficiency of 91.5% is achieved at 0.74 W.

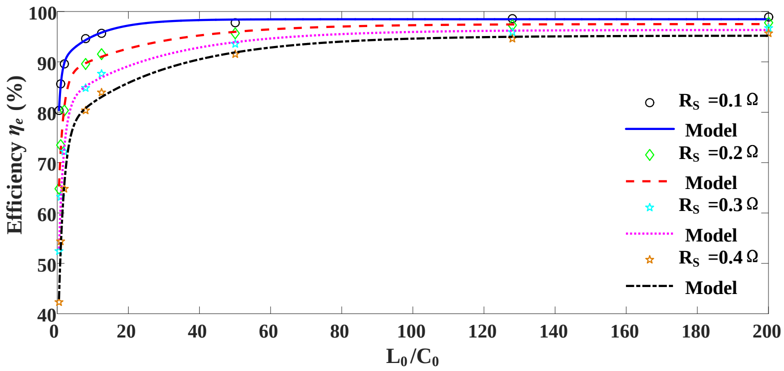

Figure 12. Theoretical efficiency η_e as a function of L_0/C_0 ratio with different R_S.

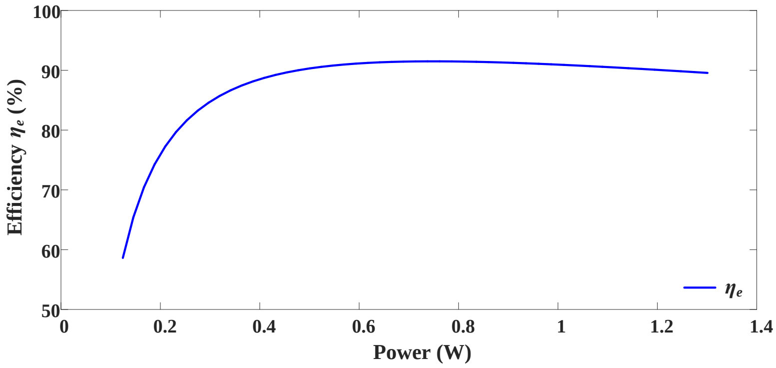

Figure 13. Theoretical efficiency η_e as a function of power at L_0/C_0 = 10 and R_S = 0.18 Ω.

3. Experimental Results

In order to verify the theoretical analysis and evaluate the equalization performance of the proposed system, a prototype for four 6200-mA·h lithium-ion cells is implemented and tested. Figure 14 shows the photographs of the experimental setup. The MOSFETs are implemented by STP220N6F7 MOSFETs with 2.4 mΩ internal resistance. The values of L_0 and C_0 are determined as 10.99 µH and 1.05 µF, respectively. The measured equivalent resistance R_S in the LC converter is about 0.18 Ω. A MicroAutoBox® II manufactured by dSPACE (Wixom, MI, USA) was used for the digital control, which can generate Pulse-Width Modulation (PWM) singles to control the MOSFETs, and receive the cell voltage information by analog-to-digital converters.

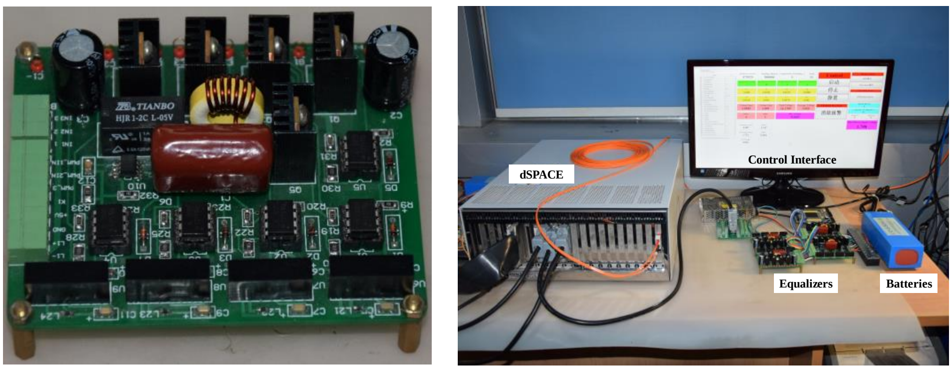

(**a**) (**b**)

Figure 14. Photographs of the implemented engineering prototype for four lithium-ion battery cells. (**a**) balancing circuit; (**b**) experimental platform.

Figure 15 shows the experimental waveforms of resonant current i_{L0} and capacitor voltage v_{C0} with different switching sequences. It can be observed that the MOSFETs are turned ON and OFF at zero current state, thus significantly reducing the switching losses. This provides the equalizer with the potential to work at higher frequencies, leading to a small size of the proposed equalizer. From Figure 15a,b, it can be seen that controlling the switching sequence can govern the direction of the balancing power flowing. This agrees well with the theoretical waveforms.

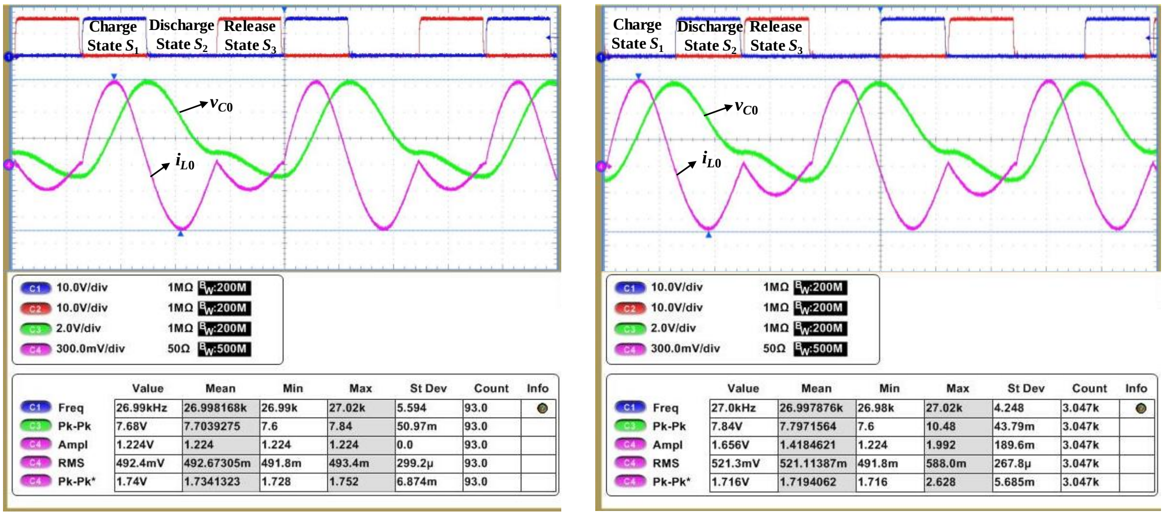

(**a**) (**b**)

Figure 15. Experimental waveforms of the proposed equalizer with different switching sequences. (**a**) energy transfer from B_0 to B_1; (**b**) energy transfer from B_1 to B_0.

Figure 16 shows the measured efficiency η_e as a function of power at $L_0/C_0 \approx 10$. When power increases from 0.226 to 0.595 W, η_e increases from 47.7% to 89.1%. When power increases from 0.595 to 0.913 W, η_e decreases slightly from 89.1% to 81.5%. This indicates that the proposed equalizer obtains a high efficiency over a wide range of output power.

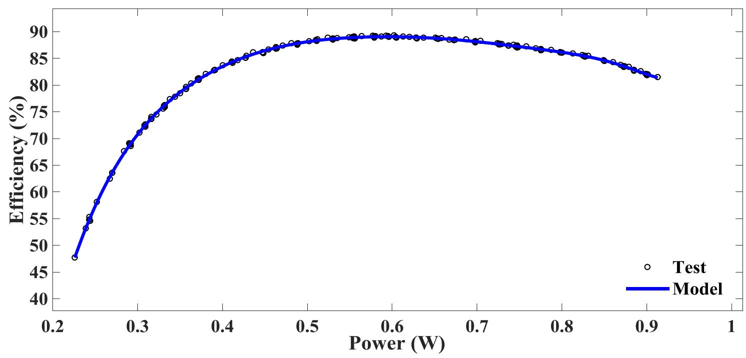

Figure 16. Measured efficiency η_e as a function of power at $L_0/C_0 \approx 10$.

Figure 17 shows the experimental results for two cells connected in series. The initial cell voltages are set as V_{B0} = 3.240 V and V_{B1} = 2.574 V, respectively. The initial maximum voltage gap is about 0.666 V. It is important to note that, in order to achieve the initial cell voltages, the battery string is not balanced until 200 s' standing. Figure 17a shows the balancing result with the classical switched capacitor. After about 8.2 h, the voltage gap between the cells is still larger than 0.109 V, which shows that the switched capacitor method cannot achieve ZVG between the two cells. Figure 17b shows the balancing result with the resonant switched capacitor. The balancing speed is increased a lot, but ZVG between cells is still not achieved after 8000 s. Figure 17c shows the balancing result with the proposed method. We observe that, after about 2056 s, the cell voltages are fully balanced to the same value of 3.171 V, showing the outstanding balancing performances (i.e., fast balancing and ZVG between cells) of the proposed scheme. Figure 17d shows the balancing result using the proposed equalizer without the release sate. It can be seen that the balancing speed becomes slow, and ZVG between cells cannot be achieved, which indicates that the release sate plays an active role in the balancing process.

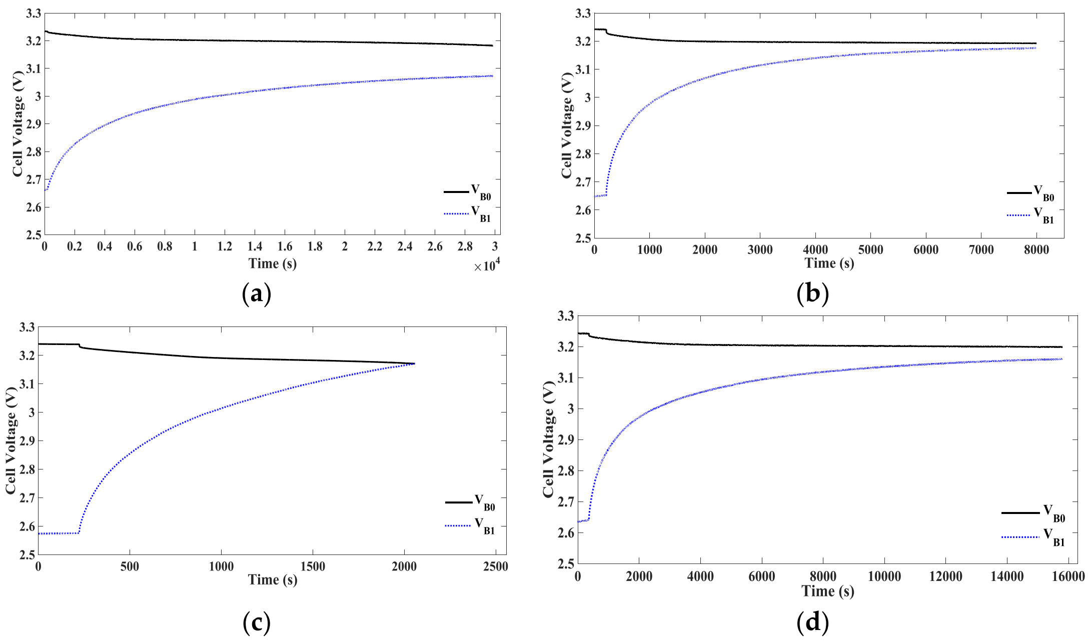

Figure 17. The voltage equalization results for two cells. (**a**) the classical SC method [10]; (**b**) the resonant SC method [15]; (**c**) the proposed method based on a LCS converter; (**d**) the proposed method based on a LCS converter without the release sate.

Figure 18 shows the experimental results for four cells connected in series. Because of the nonlinear behavior of lithium-ion batteries, it is very difficult to determine when the cell voltages are fully balanced. Thus, it is optimal to take numerous small equalization cycles to complete the energy exchange. In our method, one equalization cycle includes 10-s equalization time and 20-s standing time for the equalizer. The initial cell voltages are set as V_{B0} = 3.216 V, V_{B1} = 2.783 V, V_{B2} = 3.233 V, and V_{B3} = 3.023 V, respectively. After about 12,960 s, a balanced voltage of 3.096 V is achieved with about 178 equalization cycles.

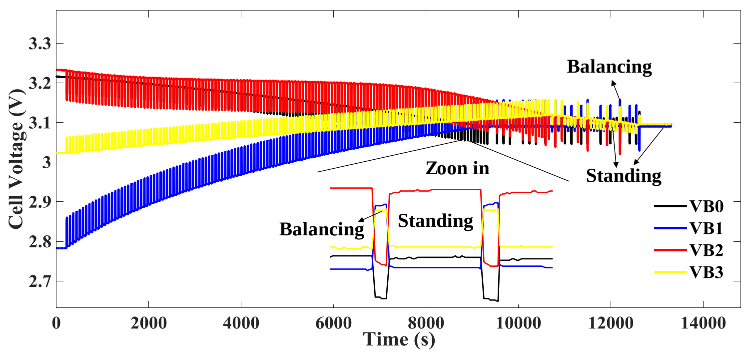

Figure 18. The voltage equalization results for four cells.

4. Comparison with Conventional Equalizers

In order to systematically evaluate the proposed scheme, Table 1 gives a comparative study with conventional battery equalizers focusing on the components, balancing speed, balancing efficiency, ZCS, ZVG among cells, and modularization. It is assumed that the battery string includes n cells connected in series, which is divided into m battery modules. Components focuses mainly on the numbers of switches (SW), resistors (R), inductors (L), capacitors (C), diodes (D), and transformers (T). The equalization speed is determined by the equalization current, the number of cells involved in balancing at the same time, and the average switching cycles to complete the charge transportation from the source cell to the target one. The balancing efficiency is evaluated according to the average energy conversion efficiency for one switching cycle and the average switching cycles to transfer energy from a cell to another one. ZCS and ZVG are evaluated according to whether the systems can achieve ZCS for all MOSFETs and obtain ZVG among cells in a battery string. Modularization is evaluated according to the implemented complexity of the equalizers when a new cell is added. These balancing performance parameters are fuzzified into three fuzzy scales, for which "H" represents the higher performance, "L" represents the lower performance, and "M" represents the medium performance, specifically, Speed (L: low, H: high), Efficiency (L: low, H: high), ZCS (L: no, H: yes), ZVG among cells (L: no, M: yes), and Modularization (L: difficult, H: easy).

All of the existing solutions provide good performance targeting. For example, the dissipative equalization method [9] has the outstanding advantages of small size, low cost, and easy implementation. However, the excess energy is consumed by the shunt resistors, resulting in a very low balancing efficiency.

SC based methods [10–14] tend to be lighter and smaller due to the absence of any magnetic components. Moreover, they have the outstanding advantages of simple control, easy modularization, and automatic equalization without cell monitoring circuits. However, the balancing efficiency is very low at a large voltage gap among cells, and the balancing speed becomes slower as the voltage gap gets smaller. In other words, these methods cannot have a high equalization efficiency and a fast balancing speed at the same time.

Inductor based methods [19–21] require only inductors and MOSFETs. Therefore, the sizes of these solutions are small, and the costs are low. These approaches can also achieve automatic equalization among cells without the requirement of cell monitoring circuits. Moreover, they are easily modularized and not limited to the numbers of battery cells in a battery string. However, they work in the hard-switching mode, and the switching loss tends to be high, leading to a low balancing efficiency. Particularly, ZVG among cells cannot be achieved due to the asymmetry of inductors and the voltage drops across power electronic devices.

Transformer-based solutions [22–32] have the inherent advantages of easy isolation, high efficiency, and simple control. However, it is definitely difficult to apply a single multi-winding transformer into a long series-connected battery string because of the mismatching, bulk size, and high complexity implementation of the multi windings. Moreover, the mismatched multi windings naturally cause the imbalance voltages during the balancing. In addition, these methods need additional components for the equalization among modules, leading to bulk size and loss related to the modularization.

By using an additional switch Q_4 connected in parallel with the LC tank, the proposed solution obtains another resonant current path to release the residual energy stored in the capacitor to the inductor, which lays the foundations to achieve the bi-directional power flow and weakens the couplings of a large voltage gap with low efficiency and a small voltage gap with slow balancing speed. From Table 1, it is apparent that the size of the proposed equalizer is comparable with the existing solutions. Moreover, it has clear advantages in terms of the balancing speed, efficiency, ZCS, ZVG, and modularization, which make the proposed system be a feasible solution for EVs in the future.

Table 1. Comparison of several battery equalizers.

Category	Components						Speed	Efficiency	ZCS	ZVG	Modularization
	SW	R	L	C	D	T					
Dissipative equalizer [9]	n	n	0	0	0	0	M	L	L	M	H
SC [10]	$2n$	0	0	$n-1$	0	0	L	M	L	L	H
Chain structure of SC [11]	$2(n+2m)$	0	0	$n+m$	0	0	L	M	L	L	L
ZCS SC [15]	$2n$	0	$n-1$	$n-1$	0	0	L	M	H	L	H
Single LC resonant converter [18]	$2(n+5m)$	0	m	m	0	0	M	M	H	L	M
Buckboost (multiple inductors) [19]	$2n$	0	$n-1$	0	0	0	M	M	L	M	H
Multiphase interleaved method [20]	$2(n-1)$	0	$n-1$	0	0	0	M	M	L	M	L
Optimized next-to-next balancing [21]	$4(n-1)$	0	$2(n-1)$	0	0	0	L	M	L	M	H
Flyback conversion [22]	$2(n-m)$	0	0	0	$2(n-m)$	m	M	M	L	M	L
Flyback or forward conversion [23]	$2n$	0	0	0	0	m	M	M	L	M	M
Forward conversion [24]	n	0	0	n	0	m	H	H	H	L	M
Wave-trap [28]	$2m$	0	n	n	n	n	M	M	H	M	L
Proposed equalizer with Q_4	$5(n-1)$	0	$n-1$	$n-1$	0	0	H	M	H	H	H
Proposed equalizer without using Q_4	$4(n-1)$	0	$n-1$	$n-1$	0	0	H	M	H	H	H

n is the number of cells in the battery string; m is the number of battery modules in the battery string; SC (Switched capacitor); ZCS (zero-current switching); LC (inductor capacitor).

5. Conclusions

In this paper, an adjacent cell-to-cell equalizer with ZCS and ZVG based on three-resonant-state SC converters is proposed. The scheme configuration, modular design, operation principles, theoretical analysis, cell-balancing performance, and comparative studies with the conventional battery equalizers are presented. The proposed scheme obtains ZCS due to the three resonant states of the LCS converter, which reduces inherently the frequency dependent switching losses, allowing efficient operation at very high switching frequencies. ZVG among cells is achieved thanks to the newly added resonant current path, which also weakens the couplings of a large voltage gap with low efficiency and a small voltage gap with slow balancing speed. A prototype with four 6200-mA·h lithium-ion cells is optimally implemented. Experiment results show that the proposed scheme exhibits good balancing performance with ZCS and ZVG, and the measured peak conversion efficiency is 89.1% at $L_0/C_0 \approx 10$.

Acknowledgments: This work was supported by the Major Scientific Instrument Development Program of the National Natural Science Foundation of China under Grant No. 61527809, the Key Project of National Natural Science Foundation of China under Grant No. 61633015, the National Natural Science Foundation of China under Grant No. 61273097, and the Major International (Regional) Joint Research Project of the National Natural Science Foundation of China (NSFC) under Grant No. 61320106011. The authors would like to thank them for their support and help. The authors would also like to thank the reviewers for their corrections and helpful suggestions.

Author Contributions: Yunlong Shang conceived this paper, designed and performed the experiments, and analyzed the data; Qi Zhang assisted the experiment and revised the paper; Naxin Cui and Chenghui Zhang revised the paper and provided some valuable suggestions.

Conflicts of Interest: The authors declare no conflict of interest.

References

1. Zhang, Y.; Xiong, R.; He, H.; Shen, W. A lithium-ion battery pack state of charge and state of energy estimation algorithms using a hardware-in-the-loop validation. *IEEE Trans. Power Electron.* **2016**. [CrossRef]
2. Sun, F.; Xiong, R.; He, H. A systematic state-of-charge estimation framework for multi-cell battery pack in electric vehicles using bias correction technique. *Appl. Energy* **2016**, *162*, 1399–1409. [CrossRef]
3. Xiong, R.; Sun, F.; Gong, X.; Gao, C. A data-driven based adaptive state of charge estimator of lithium-ion polymer battery used in electric vehicles. *Appl. Energy* **2014**, *113*, 1421–1433. [CrossRef]
4. Xia, B.; Mi, C. A fault-tolerant voltage measurement method for series connected battery packs. *J. Power Source* **2016**, *308*, 83–96. [CrossRef]
5. Lu, L.; Han, X.; Li, J.; Hua, J.; Ouyang, M. A review on the key issues for lithium-ion battery management in electric vehicles. *J. Power Source* **2013**, *226*, 272–288. [CrossRef]
6. Xiong, R.; Sun, F.; Chen, Z.; He, H. A data-driven multi-scale extended Kalman filtering based parameter and state estimation approach of lithium-ion polymer battery in electric vehicles. *Appl. Energy* **2014**, *113*, 463–476. [CrossRef]
7. Lozano, J.G.; Cadaval, E.R. Battery equalization active methods. *J. Power Source* **2014**, *246*, 934–949. [CrossRef]
8. Battery. Available online: http://batteryuniversity.com/learn/article/electric_vehicle_ev (accessed on 8 February 2017).
9. Gallardo-Lozano, J.; Romero-Cadaval, E.; Milanes-Montero, M.I.; Guerrero-Martinez, M.A. A novel active battery equalization control with on-line unhealthy cell detection and cell change decision. *J. Power Source* **2015**, *299*, 356–370. [CrossRef]
10. Pascual, C.; Krein, P.T. Switched capacitor system for automatic series battery equalization. In Proceedings of the IEEE 1997 Applied Power Electronics Conference, Atlanta, GA, USA, 23–27 February 1997; pp. 848–854.
11. Kim, M.Y.; Kim, C.H.; Kim, J.H.; Moon, G.W. A chain structure of switched capacitor for improve cell balancing speed of lithium-ion batteries. *IEEE Trans. Ind. Electron.* **2014**, *61*, 3989–3999. [CrossRef]
12. Shang, Y.L.; Xia, B.; Lu, F.; Zhang, C.H.; Cui, N.X.; Mi, C. A switched-coupling-capacitor equalizer for series-connected battery strings. *IEEE Trans. Power Electron.* **2016**. [CrossRef]
13. Ye, Y.; Cheng, K.W.E. An automatic switched-capacitor cell balancing circuit for series-connected battery strings. *Energies* **2016**, *9*, 138. [CrossRef]
14. Ye, Y.; Cheng, K.W.E. Modeling and analysis of series-parallel switched-capacitor voltage equalizer for battery/supercapacitor strings. *IEEE J. Emerg. Sel. Top. Power Electron.* **2015**, *3*, 977–983. [CrossRef]

15. Ye, Y.; Cheng, K.W.E.; Yeung, Y.P.B. Zero-current switching switched-capacitor zero-voltage-gap automatic equalization system for series battery string. *IEEE Trans. Power Electron.* **2012**, *27*, 3234–3242.
16. Shang, Y.; Zhang, C.; Cui, C.N.; Guerrero, J.M. A cell-to-cell battery equalizer with zero-current switching and zero-voltage gap based on quasi-resonant LC converter and boost converter. *IEEE Trans. Power Electron.* **2015**, *30*, 3731–3747. [CrossRef]
17. Shang, Y.; Zhang, C.; Cui, C.N.; Guerrero, J.M.; Sun, K. A crossed pack-to-cell equalizer based on quasi-resonant LC converter with adaptive fuzzy logic equalization control for series-connected lithium-ion battery strings. In Proceedings of the IEEE 2015 Applied Power Electronics Conference, Charlotte, NC, USA, 15–19 March 2015; pp. 1685–1692.
18. Lee, K.; Chung, Y.; Sung, C.-H.; Kang, B. Active cell balancing of li-ion batteries using LC series resonant circuit. *IEEE Trans. Ind. Electron.* **2015**, *62*, 5491–5501. [CrossRef]
19. Kim, M.-Y.; Kim, J.-H.; Moon, G.-W. Center-cell concentration structure of a cell-to-cell balancing circuit with a reduced number of switches. *IEEE Trans. Power Electron.* **2014**, *29*, 5285–5297. [CrossRef]
20. Mestrallet, F.; Kerachev, L.; Crebier, J.-C.; Collet, A. Multiphase interleaved converter for lithium battery active balancing. *IEEE Trans. Power Electron.* **2014**, *29*, 2874–2881. [CrossRef]
21. Phung, T.H.; Collet, A.; Crebier, J.-C. An optimized topology for next-to-next balancing of series-connected lithium-ion cells. *IEEE Trans. Power Electron.* **2014**, *29*, 4603–4613. [CrossRef]
22. Imitiaz, A.M.; Khan, F.H. "Time shared flyback converter" based regenerative cell balancing technique for series connected li-ion battery strings. *IEEE Trans. Power Electron.* **2013**, *28*, 5960–5975. [CrossRef]
23. Chen, Y.; Liu, X.; Cui, Y.; Zou, J.; Yang, S. A multi-winding transformer cell-to-cell active equalization method for lithium-ion batteries with reduced number of driving circuits. *IEEE Trans. Power Electron.* **2016**, *31*, 4916–4929. [CrossRef]
24. Li, S.; Mi, C.; Zhang, M. A high-efficiency active battery-balancing circuit using multiwinding transformer. *IEEE Trans. Ind. Appl.* **2013**, *49*, 198–207. [CrossRef]
25. Uno, M.; Kukita, A. Double-switch equalizer using parallel-or series-parallel-resonant inverter and voltage multiplier for series-connected supercapacitors. *IEEE Trans. Power Electron.* **2014**, *29*, 812–828. [CrossRef]
26. Anno, T.; Koizumi, H. Double-input bidirectional DC/DC converter using cell-voltage equalizer with flyback transformer. *IEEE Trans. Power Electron.* **2015**, *30*, 2923–2934. [CrossRef]
27. Hua, C.; Fang, Y.-H. A charge equalizer with a combination of APWM and PFM control based on a modified half-bridge converter. *IEEE Trans. Power Electron.* **2016**, *31*, 2970–2979. [CrossRef]
28. Arias, M.; Sebastián, J.; Hernando, M.; Viscarret, U.; Gil, I. Practical application of the wave-trap concept in battery-cell equalizers. *IEEE Trans. Power Electron.* **2015**, *30*, 5616–5631. [CrossRef]
29. Lim, C.-S.; Lee, K.-J.; Ku, N.-J.; Hyun, D.-S.; Kim, R.-Y. A modularized equalization method based on magnetizing energy for a series-connected Lithium-ion battery string. *IEEE Trans. Power Electron.* **2014**, *29*, 1791–1799. [CrossRef]
30. Kim, C.-H.; Kim, M.-Y.; Moon, G.-W. A modularized charge equalizer using a battery monitoring IC for series-connected Li-ion battery strings in electric vehicles. *IEEE Trans. Power Electron.* **2013**, *28*, 3779–3787. [CrossRef]
31. Park, H.-S.; Kim, C.-H.; Park, K.-B.; Moon, G.-W.; Lee, J.-H. Design of a charge equalizer based on battery modularization. *IEEE Trans. Veh. Technol.* **2009**, *58*, 3216–3223. [CrossRef]
32. Xu, A.; Xie, S.; Liu, X. Dynamic voltage equalization for series-connected ultracapacitors in EV/HEV applications. *IEEE Trans. Veh. Technol.* **2009**, *58*, 3981–3987.
33. Cervera, A.; Evzelman, M.; Mordehai Peretz, M.; Ben-Yaakov, S. A high efficiency resonant switched capacitor converter with continuous conversion ratio. *IEEE Trans. Power Electron.* **2014**, *30*, 1373–1382. [CrossRef]
34. Blumenfeld, A.; Cervera, A.; Mordechai Peretz, M. Enhanced differential power processor for PV systems: Resonant switched-capacitor gyrator converter with local MPPT. *IEEE J. Emerg. Sel. Top. Power Electron.* **2014**, *2*, 883–892. [CrossRef]
35. Dong, B.; Li, Y.; Han, Y. Parallel architecture for battery charge equalization. *IEEE Trans. Power Electron.* **2015**, *30*, 4906–4913. [CrossRef]